ADVANCED FUNCTIONAL MATERIALS
www.afm-journal.de

Inkjet Printed Disposable High-Rate On-Paper Microsupercapacitors

*Zheng Li, Virginia Ruiz, Viktoriia Mishukova, Qiansu Wan, Haomin Liu, Han Xue, Ying Gao, Gaolong Cao, Yuanyuan Li, Xiaodong Zhuang, Jonas Weissenrieder, Shi Cheng, and Jiantong Li**

On-paper microsupercapacitors (MSCs) are a key energy storage component for disposable electronics that are anticipated to essentially address the increasing global concern of electronic waste. However, nearly none of the present on-paper MSCs combine eco-friendliness with high electrochemical performance (especially the rate capacity). In this work, highly reliable conductive inks based on the ternary composite of poly(3,4-ethylenedioxythiophene): poly(styrenesulfonate) (PEDOT:PSS), graphene quantum dots and graphene are developed for scalable inkjet printing of compact (footprint area ≈ 20 mm^2) disposable MSCs on commercial paper substrates. Without any post treatment, the printed patterns attain a sheet resistance as low as 4 Ω □$^{-1}$. The metal-free all-solid-state MSCs exhibit a maximum areal capacitance > 2 mF cm^{-2} at a high scan rate of 1000 mV s^{-1}, long cycle life (>95% capacitance retention after 10 000 cycles), excellent flexibility, and long service time. Remarkably, the "totally metal-free" MSC arrays are fully inkjet printed on paper substrates and also exhibit high rate performance. The life cycle assessment indicates that these printed devices have much lower eco-toxicity and global warming potential than other on-paper MSCs.

1. Introduction

While the rapid growth of portable electronics, wearable electronics and Internet of Things has brought great benefits to people's everyday life, the accompanying generation of large-scale electronic waste is becoming a global concern.[1] Eco-friendly and disposable electronics, which at the end of the life cycle can be thrown away in the trash without noticeable impact on the environment, are envisioned as the most effective solution to the growing issue of electronic waste.[1,2] Among various disposable electronic components, on-paper microsupercapacitors (MSCs)[1–4] have attracted plenty of research interest. In general, as a type of microscale energy storage components (typically in planar interdigitated structure with feature size < 1 mm and footprint area < 1 cm^2),[5] MSCs have great potential for miniaturized electronics and self-powered smart systems because of their high power density, fast charging rate, and long cycle life. On-paper MSCs are of even higher interest thanks to the low cost, eco-friendliness and renewability of the paper substrates. Recently, various efforts have been made to develop advanced materials and patterning approaches for the fabrication of paper MSCs. However, in general, the eco-friendliness and disposability of the paper MSCs are achieved at the expense of electrochemical performance, especially the rate capacity. For example, disposable on-paper MSCs based on 3D printed purely carbon-based materials,[2] laser-induced molybdenum carbide/graphene composites,[4] and inkjet/extrusion

Z. Li, V. Mishukova, Q. Wan, H. Liu, H. Xue, S. Cheng, J. Li
School of Electrical Engineering and Computer Science
KTH Royal Institute of Technology
Electrum 229, Kista SE-164 40, Sweden
E-mail: jiantong@kth.se

V. Ruiz
CIDETEC
Basque Research and Technology Alliance (BRTA)
Paseo Miramón 196, Donostia-San Sebastián E-20014, Spain

The ORCID identification number(s) for the author(s) of this article can be found under https://doi.org/10.1002/adfm.202108773.

DOI: 10.1002/adfm.202108773

Y. Gao, Y. Li
Wallenberg Wood Science Center
Department of Fiber and Polymer Technology
KTH Royal Institute of Technology
Stockholm SE-10044, Sweden

G. Cao, J. Weissenrieder
School of Engineering Sciences
Department of Applied Physics
AlbaNova
KTH Royal Institute of Technology
Stockholm SE-106 91, Sweden

X. Zhuang
The Soft2D Lab
State Key Laboratory of Metal Matrix Composites
Shanghai Key Laboratory of Electrical Insulation and Thermal Ageing
School of Chemistry and Chemical Engineering
Shanghai Jiao Tong University
Shanghai 200240, China

printed MXene[6] have been fabricated with high capacitance at low scan rates while their performance significantly degrades at higher scan rates over 100 mV s^{-1}. High-rate performance generally necessitates electrodes with large accessible surface area (to shorten the transport path of the electrolyte ions)[7] and low electrical resistance (to promote the electron transfer),[8] and also electrolytes with high ionic conductance. For most on-paper MSCs, although the non-metal (usually carbon-based) electrode materials are superior in capacitive properties, their relatively low electrical conductivity significantly inhibits the high rate performance. In order to increase the rate capacity to a high scan rate over 1000 mV s^{-1}, metal current collectors are often needed, such as gold current collectors deposited through magnetron sputtering,[3] nickel current collectors fabricated through matrix-assisted catalytic printing and electroplating,[9] and inkjet printed silver current collectors.[10] However, the use of metal current collectors significantly increases the complexity and cost of the processing, and more importantly, severely sacrifices the eco-friendliness and disposability of the entire devices. Therefore, highly desired are those on-paper MSCs that can achieve high rate performance while being fully based on disposable (metal-free or all-carbon) materials.

On top of the development of active materials, attention should also be paid to the eco-friendliness and sustainability of the fabrication processes. In spite of the disposability of the final devices, their fabrication processes may have to rely on toxic chemicals or solvents, involve considerable waste of precious functional materials, and/or release toxic by-products.[3] In this regard, inkjet printing is regarded as a sustainable technique due to its combination of multiple merits, such as purely additive processing, direct (mask-free) patterning, relatively high resolution, minimized material waste, good scalability, and excellent compatibility with versatile active materials and substrates.[11] In particular, paper is a superior substrate for inkjet printing thanks to its hierarchical structure of cellulose fibers which leads to porous and rough surface texture and multiscale capillary for easy absorption of the ink solvents and hence quick formation of the printed patterns.[3] However, several challenges are still foreseen for inkjet printing of high-rate on-paper MSCs. First, inkjet printing excels in fabricating high-resolution thin patterns whereas MSCs prefer thick electrode patterns to increase the areal performance.[5,12] As a result, highly stable and reliable inks[13] should be developed to enable multiple printing (overwriting) passes to increase the electrode thickness without causing electrical shorts between the two separate electrodes.[14] Second, due to the strong absorption of paper, aggressive or nonvolatile solvents should be avoided in the inks to prevent the substrates from mechanical deformation. Last, paper is vulnerable to many post-treatments, such as high-temperature sintering which is necessary for many high-performance electrodes fabrication. This makes it difficult to inkjet print highly conductive patterns on paper substrates[3] to ensure high rate performance of the MSCs.

In this work, we develop a simple yet highly-reliable inkjet printing technique for scalable fabrication of disposable high-rate paper MSCs. The key point is the successful formulation of binder-free and eco-friendly conductive inks based on the ternary composite (denoted as PDG hereafter) of poly(3,4-ethylenedioxythiophene): poly(styrenesulfonate) (PEDOT:PSS), graphene quantum dots (GQDs) and electrochemically exfoliated graphene (EEG) dispersed in the mild water/ethylene glycol (EG) solvent mixture. In the literature, various inkjet printing techniques[10,15–20] of PEDOT:PSS have been developed and widely used in flexible and stretchable electronics due to its tunable electrical conductivity, high flexibility, and good biocompatibility.[21] However, insulating additives and/or aggressive solvents[17,20] are typically used to stabilize the PEDOT:PSS inks at the expense of electrical conductance or eco-friendliness. Accordingly, the inkjet printed PEDOT:PSS-based MSCs or transparent supercapacitors[10,16,18,19] often suffer from low rate performance or the need of metal current collectors. On the other hand, GQDs have recently received tremendous interest in supercapacitor applications due to their excellent rate capability (over 1000 V s^{-1}, with metal current collectors).[22,23] In this work, we demonstrate that, along with EEG, specific GQDs can simultaneously stabilize PEDOT:PSS in the ink solvents and improve the rate performance of the printed MSCs. The high stability of the inks enables efficient and reliable printing of interdigitated MSCs (with footprint area as small as 20 mm^2 and inter-finger gap as narrow as 300 μm) at large electrode thickness up to ≈10 μm. Without sintering or any other post-treatments (i.e., merely after naturally drying in air), the printed PDG patterns can readily attain a sheet resistance < 10 Ω $\square^{-1}$ on paper substrates. Free from metal current collectors, the all-solid-state on-paper MSCs attain a large areal capacitance >2 mF cm^{-2} at a scan rate of 1000 mV s^{-1}. Furthermore, small-scale metal-free MSC arrays (four cells connected in series or parallel) are fully printed on paper substrates with PDG as both the MSC electrodes and interconnect to enable fast charging/discharging at a high rate of 1000 mV s^{-1}.

2. Results and Discussion

The challenge to develop inkjet printing techniques for metal-free high-rate on-paper MSCs lies in the effective dispersion of conductive electrode materials in the inkjet printable solvents without using any insulating binders. The water-soluble conducting polymer PEDOT:PSS is a good candidate for the electrode material. In this work, an EG/water mixture is used as solvent for the PDG inks (**Figure 1**a). On the one hand, the mixture is frequently used in inkjet printing inks for uniform patterning due to its effective prevention of the well-known coffee-ring effects[24] and its negligible impact on the paper substrates. On the other hand, EG is an excellent dopant for PEDOT:PSS which can significantly improve the electrical conductivity from < 1 S cm^{-1} to > 100 S cm^{-1}.[21] However, pure PEDOT:PSS (at the concentration of 3 mg mL^{-1}) is not stable in the EG/water solvent, as confirmed by a low zeta potential of −19 mV (Figure 1b), large particle size and high polydispersity of the size distribution in the dynamic light scattering (DLS) characterization (Figure 1c). This can be ascribed to the EG-induced phase separation of the PEDOT:PSS copolymer.[21] The water-soluble PSS chains are dissolved into the EG solution while the remaining PEDOT chains aggregate to form large particles, which severely decreases the ink stability. Nevertheless, we have found that after adding a specific type of GQDs (0.8 mg mL^{-1}, synthesized via pyrolysis of citric acid),[25]

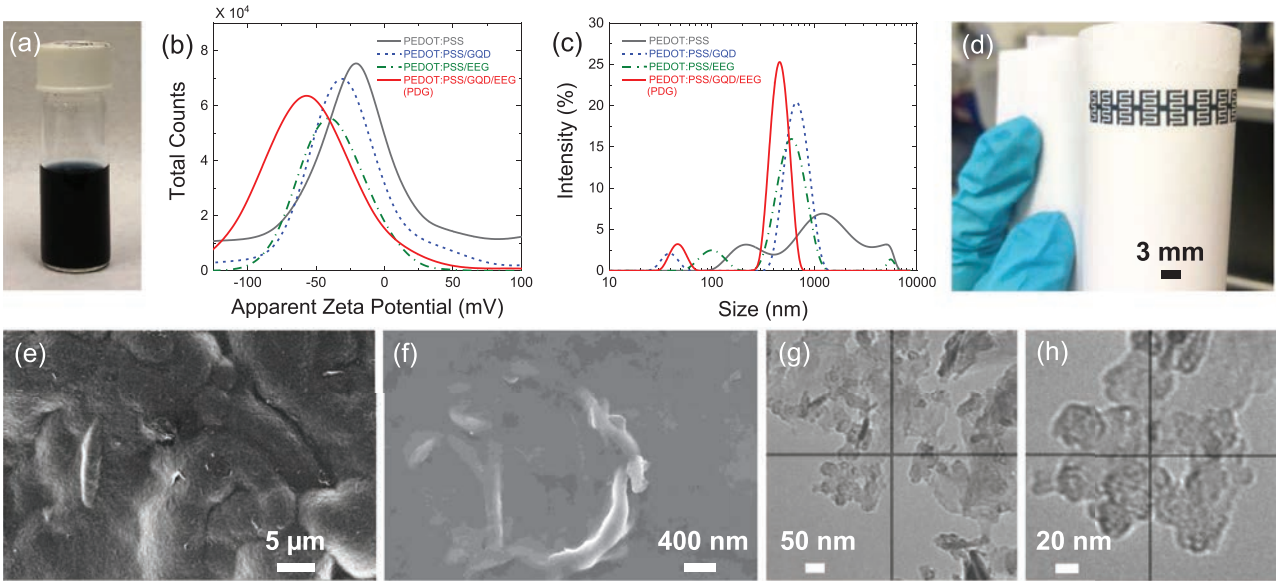

Figure 1. Characterization of the PDG inks. a) Photograph of a PDG ink, b) zeta potential and c) DLS particle size distribution of PEDOT:PSS, PEDOT:PSS/GQD, PEDOT:PSS/EEG, and the ternary PDG dispersions in water/EG mixture (volume ratio 2:1), d) photograph of printed PDG patterns on a photo paper, e,f) SEM images of the printed PDG patterns on a photo paper, g,h) TEM images of the PDG ink.

the binary PEDOT:PSS/GQD composite attains moderate stability[26] in the EG/water solvent with a more negative zeta potential of −32 mV (Figure 1b) and smaller particle size and lower polydispersity (Figure 1c). The GQDs have lateral size about 10 nm and thickness around 1–3 nm[25] (also indicated as the circular particles in the TEM images in Figure 1g,h). They contain abundant hydroxyl and carboxylate edge groups, as revealed by the main bands in the FTIR spectra at 3300, 1560, and 1384 cm^{-1}, corresponding to the O-H stretch, and the asymmetric and symmetric stretch in carboxylates, respectively (Figure S1a, Supporting Information). These groups make the GQDs highly stable in the water/EG mixture under various pH environments (Figure S1b, Supporting Information) and can stabilize PEDOT:PSS in the binary dispersions: since both GQDs and PEDOTs are rich in π bonds, the PEDOT chains can readily attach to the GQD basal planes through strong π–π interactions, and meanwhile the PSS chains can attach to the GQD edges through hydrophilic interactions.[27] As a result, the stability of PEDOT:PSS in the EG/water solvent can be greatly improved even after the separation between the PEDOT and PSS chains. In addition, the stability of the binary PEDOT:PSS/EEG inks is also investigated, where the EEG concentration is ≈0.1 mg mL^{-1} (Table S1, Supporting Information). Similar to GQDs, EEG is also rich in π bonds and contains a certain amount of hydrophilic oxygen groups on the flake edges (≈5.5% atom of oxygen),[28] but with much larger flake size (mostly > 1 µm, Figure 1e,f). Again, the PEDOT chains can attach to the EEG flakes, while the PSS chains may attach to the EEG flake edges to effectively prevent the aggregation of PEDOT chains and results in more stable PEDOT:PSS/EEG inks with a zeta potential of −37 mV (Figure 1b). However, the binary inks cannot effectively prevent the aggregation between the EEG flakes (or PEDOT-coated EEG flakes) due to their strong π–π interaction, as indicated by the high polydispersity and large particle size (one peak at the position around 5 µm) in Figure 1c. Large particles will cause nozzle clogging during inkjet printing and severely reduce the jetting reliability. To address this issue, the highly stable[26] ternary PEDOT:PSS/GQD/EEG (PDG) inks (with the same concentration of each component as in other inks, as listed in Table S1, Supporting Information) are prepared with zeta potential about −55 mV (Figure 1b) and the smallest particle size and lowest polydispersity of all the prepared inks (Figure 1c). The mechanism could be ascribed to the attachment (through π–π interaction) of GQDs at the PEDOT-coated EEG flakes (Figure 1h), which increases the hydrophilicity of EEG and prevents the inter-flake aggregation thanks to the significantly higher oxygen content (44.8% atom)[25] in GQDs than that in EEG (5.5% atom).[28]

The stable ternary PDG inks exhibit excellent jetting performance (Figure S2, Supporting Information) and enable efficient printing of the PDG patterns at a high resolution of ≈50 µm (Figure S3, Supporting Information) on various paper substrates (Figure 1d-f and S4). In particular, due to the strong absorption of the paper substrates, it is feasible to print the inks at a small drop spacing of 10 µm and multiple printing passes (layers) to fabricate interdigitated MSC electrodes (**Figure 2**a) of inter-finger gap ≈ 300 µm and thickness up to 9 µm without electrical short. As shown in Figure 2b, each printing pass produces a thickness as large as ≈0.4 µm. The patterns are uniform and free from the coffee-ring effect (Figure S5, Supporting Information).[29] Their sheet resistance (Figure 2b and Figure S6, Supporting Information) scales well with the printing passes, from 23 Ω $\square^{-1}$ for 5 passes to 4 Ω $\square^{-1}$ for 25 passes, corresponding to the electrical conductivity ranging from 214 to 278 S cm^{-1}. Without any post-treatment, the sheet resistance of the printed patterns is significantly lower than that of doped PEDOT:PSS films (mostly > 30 Ω $\square^{-1}$) published in the literature.[21] Certainly, one should note that our present multi-layer printing process is restricted to thick paper substrates (such as carton paper). If thick patterns on thin paper substrates are

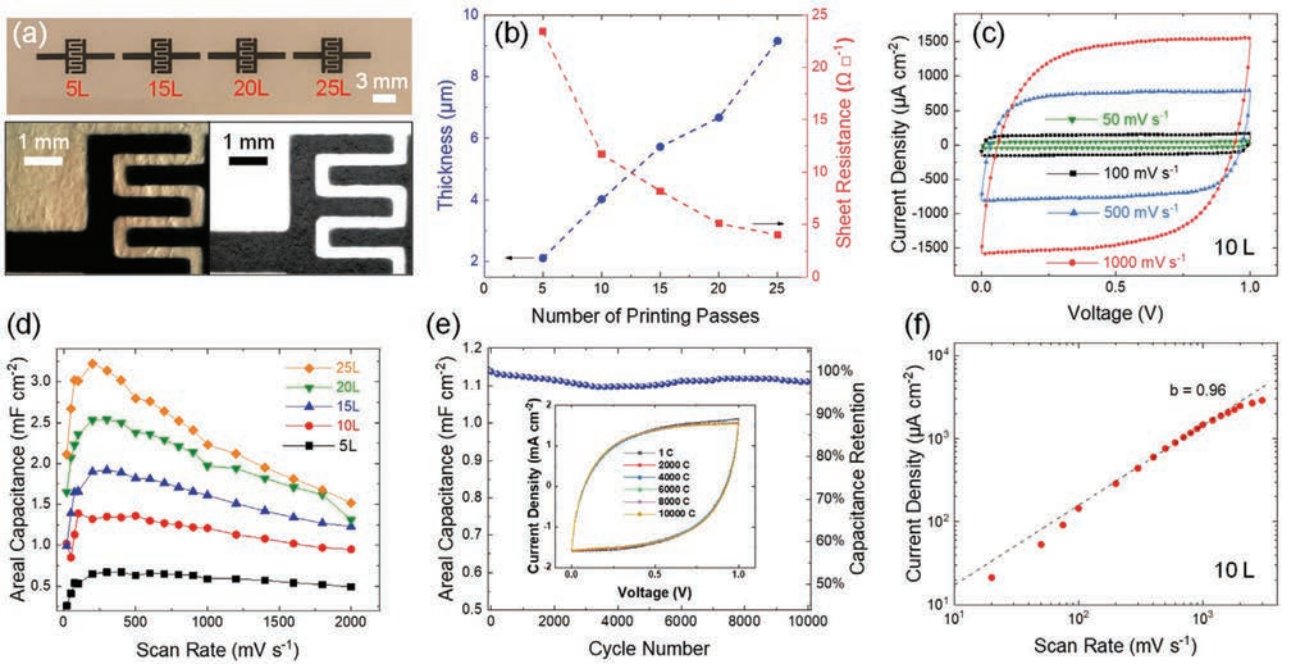

Figure 2. Electrochemical characterization of the printed on-paper MSCs. a) (upper) Photograph of the printed MSC electrodes on carton paper with different printing passes, and (lower) micrographs of the electrodes (10 printing passes) of a MSC with focus on the paper substrate (left) and the top of the PDG patterns (right), respectively, b) the dependence of the thickness and sheet resistance on the number of printing passes, c) CV curves for the device printed with 10 passes at different scan rates, d) the areal capacitance extracted from the CV curves against scan rates for all the devices, e) the areal capacitance and capacitance retention of a MSC (printed with 10 passes) at a scan rate of 1000 mV s^{-1} after various cycles, (inset) CV curves after different number of cycles, f) log–log plot of the charging current density (at the voltage of 0.5 V) against scan rates for a MSC printed with 10 passes. The dash line fits the data within the scan rate region from 20 to 1200 mV s^{-1}.

needed, the ink solvent may deform the substrates and hence cause difficulty in inter-layer alignment. Nevertheless, an in situ photonic annealing process[30] could be used to quickly evaporate the ink solvents and avoid substrate deformation, so as to enable thick patterns on thin paper substrates.

Therefore, our fabrication of paper MSCs is as simple as a single process of inkjet printing of the PDG electrodes followed by drop casting of the printable gel electrolytes, the mixture of poly(styrenesulfonic acid) (PSSH) and phosphoric acid.[14] The cyclic voltammetry (CV) test (Figure 2c) indicates that the MSCs (with 10 printing passes) exhibit excellent capacitive behavior with nearly perfect rectangularity in the CV curves at all the scan rates up to 1000 mV s^{-1}. Even at the high scan rate of 1000 mV s^{-1}, the areal capacitance is as high as ≈1.2 mF cm^{-2}. When the number of printing passes increases (up to 25), the MSCs still exhibit excellent capacitive behavior at a moderate scan rate of 100 mV s^{-1} (Figure S7a, Supporting Information) and there is only a minor deformation in the CV curves at the high scan rate of 1000 mV s^{-1} (Figure S7b, Supporting Information). The areal capacitance of the paper MSCs increases with the number of printing passes (Figure 2d), with the highest value of 3.2 mF cm^{-2} for the 25-layer devices at the scan rate of 200 mV s^{-1}. At high scan rates between 200 and 1200 mV s^{-1}, the capacitance is almost independent of the scan rate for the thin electrodes (≤10 layers) and decreases slowly with the increasing scan rate for thick electrodes (>10 layers), suggesting good rate capacity. To further confirm the high-rate performance, we plot in Figure 2f and Figure S8, Supporting Information the dependence of charging current density i at the voltage of 0.5 V on the scan rate ν, in terms of the assumed power law of $i \approx \nu^b$ with b being the exponent, respectively. A high-rate capacitive storage mechanism leads to $b \approx 1$ while a reduction to $b \approx 0.5$ corresponds to a slow diffusion-limited storage process.[7,12] For our paper MSCs at scan rates between 200 and 2000 mV s^{-1}, $b > 0.9$ is observed for all the electrodes with ≤ 15 printing passes. Even for MSCs with the thickest electrodes (25 passes), b is still above 0.8 (Figure S8, Supporting Information). These results confirm the fast capacitive storage mechanism in all the paper MSCs. This can be ascribed to the presence of GQDs in the electrodes,[23] the high electrical conductance of the printed PDG electrodes and the large ionic conductivity of the PSSH/H_3PO_4 electrolytes. The polyelectrolyte PSSH is adopted as solid-state electrolyte for our disposable paper MSCs mainly because of its environmental amicability, durability, and high ionic conductivity.[31] In particular, after being mixed with phosphoric acid, PSSH can remain in gel form (Figure S9, Supporting Information) and retain the high ionic conductivity in air (i.e., without any encapsulation) for a long time.[14] As shown in Figure S9, Supporting Information, after 2 months, the paper MSCs still retain performance comparable to the fresh devices at the high scan rate of 1000 mV s^{-1}. Even after 4 months, 84% capacitance can still be retained. These merits of the electrolyte avoid the need of encapsulation, simplify the device fabrication, and enhance the disposability. The paper MSCs also have long cycle life. After 10 000 cycles at the high scan rate of 1000 mV s^{-1}, their CV curves still

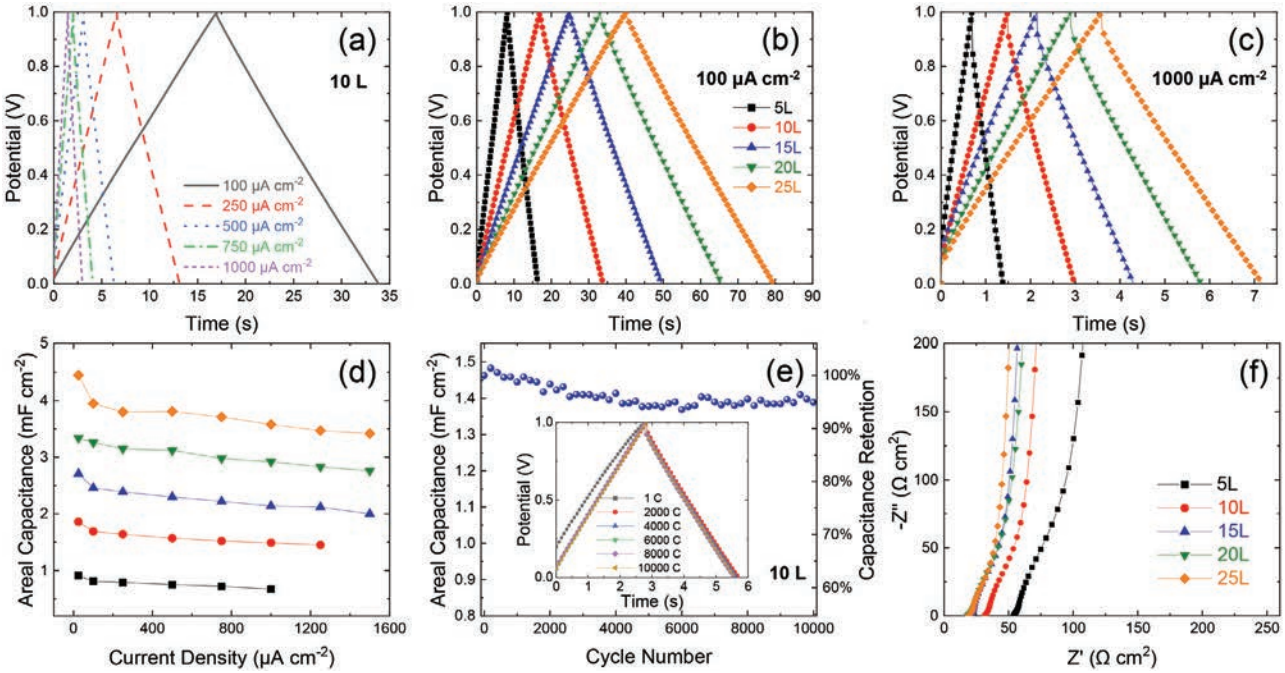

Figure 3. Galvanostatic charge-discharge (GCD) performance of printed paper MSCs. a) GCD curves for a MSC (10 printing passes) at various current densities, b,c) GCD curves of MSCs with different printing passes at a current density of b) 100 μA cm^{-2} and c) 1000 μA cm^{-2}, d) areal capacitance extracted from the GCD curves against the current density for MSCs with different printing passes, e) the areal capacitance and capacitance retention of a MSC (10 printing passes) against cycle number, (inset) GCD curves after different number of cycles, f) Nyquist plots for the MSCs with different printing passes at high frequency region.

retain excellent rectangularity with 97.6% capacitance retention (Figure 2e).

Different from other supercapacitors, at low scan rates < 200 mV s^{-1}, the areal capacitance of our PDG-based MSCs increases with the increasing scan rate, and is lower than that at 200 mV s^{-1} (Figure 2d). Such low-rate decay seems not related to the test sequence or the environmental humidity (Figure S10, Supporting Information) as well studied in other research,[32] but could be attributed to the interaction between the electrolyte and GQDs. To clarify this point, we used the same process as in our previous work[33] (drop casting of electrode inks on paper substrates following by laser patterning) to fabricate four different MSCs of the same geometry (Figure S11, Supporting Information) with pure PEDOT:PSS, PEDOT:PSS/GQD, PEDOT:PSS/EEG, and PDG as electrodes, respectively. The low-rate decay only occurs in the MSCs containing GQDs in the electrodes, but not for that of the pure PEDOT:PSS electrode. On the other hand, at high scan rates, the capacitance of the pure PEDOT:PSS-based MSC significantly decreases with the scan rate, whereas that for GQD- or EEG-containing electrodes does not. Therefore, besides the improvement of ink stability, the addition of GQDs and EEG also increases the high-rate performance of the printed MSCs. The reason could be that the uniform coating of PEDOT:PSS on the large EEG flakes (Figure 1f, their presence in the inkjet printed PDG is also confirmed by the Raman spectra in Figure S12, Supporting Information) greatly shortens the electron transport paths and increases the electrical conductivity. The large specific surface area, enriched defects, and tremendous accessible edges of GQDs facilitate the access of electrolyte ions and shorten the ion diffusion length.[23] Therefore, the synergy between EEG and GQDs significantly improves the high rate performance of the PEDOT:PSS-based MSCs.

The symmetrical and triangular galvanostatic charge-discharge (GCD) curves in **Figure 3**a–c even at high current density up to 1000 μA cm^{-2} further confirm the excellent capacitive behavior and rate capacity of the on-paper MSCs. At the moderate current density of 100 μA cm^{-2} (Figure 3b), the GCD curves do not indicate any visible IR drop (the voltage drop at the beginning of each discharge curve)[34] for all the paper MSCs. Only at the very high current density of 1000 μA cm^{-2} (Figure 3c), there is a small IR drop of 0.08 V. These imply the very low overall resistance and high power density of the MSCs.[34] The capacitance does not delay significantly with increasing current density. The areal capacitance extracted from GCD curves (Figure 3d) is up to 4.5 mF cm^{-2} for the MSC of 25-pass electrodes at the low current density of 25 μA cm^{-2}. When the current density increases to 1500 μA cm^{-2}, the areal capacitance is still as large as 3.4 mF cm^{-2}. Furthermore, after 10 000 GCD cycles at a high current density of 500 μA cm^{-2}, the MSCs (with 10 printing passes) retain 94.9% of the initial capacitance (Figure 3e), comparable to the results of the CV test (Figure 2e). The low resistance of the paper MSCs can be further confirmed by the electrochemical impedance spectroscopy (EIS) in Figure 3f where the equivalent series resistance is <20 Ω cm^2 for thick electrodes (>10 passes). In addition, in the Nyquist plot (Figure 3f) the 45° Warburg diffusion element does not appear in the mid-frequency region, implying fast ion diffusion in the paper MSCs.[7,12,28] The impedance phase angle plot (Figure S7c, Supporting Information) shows

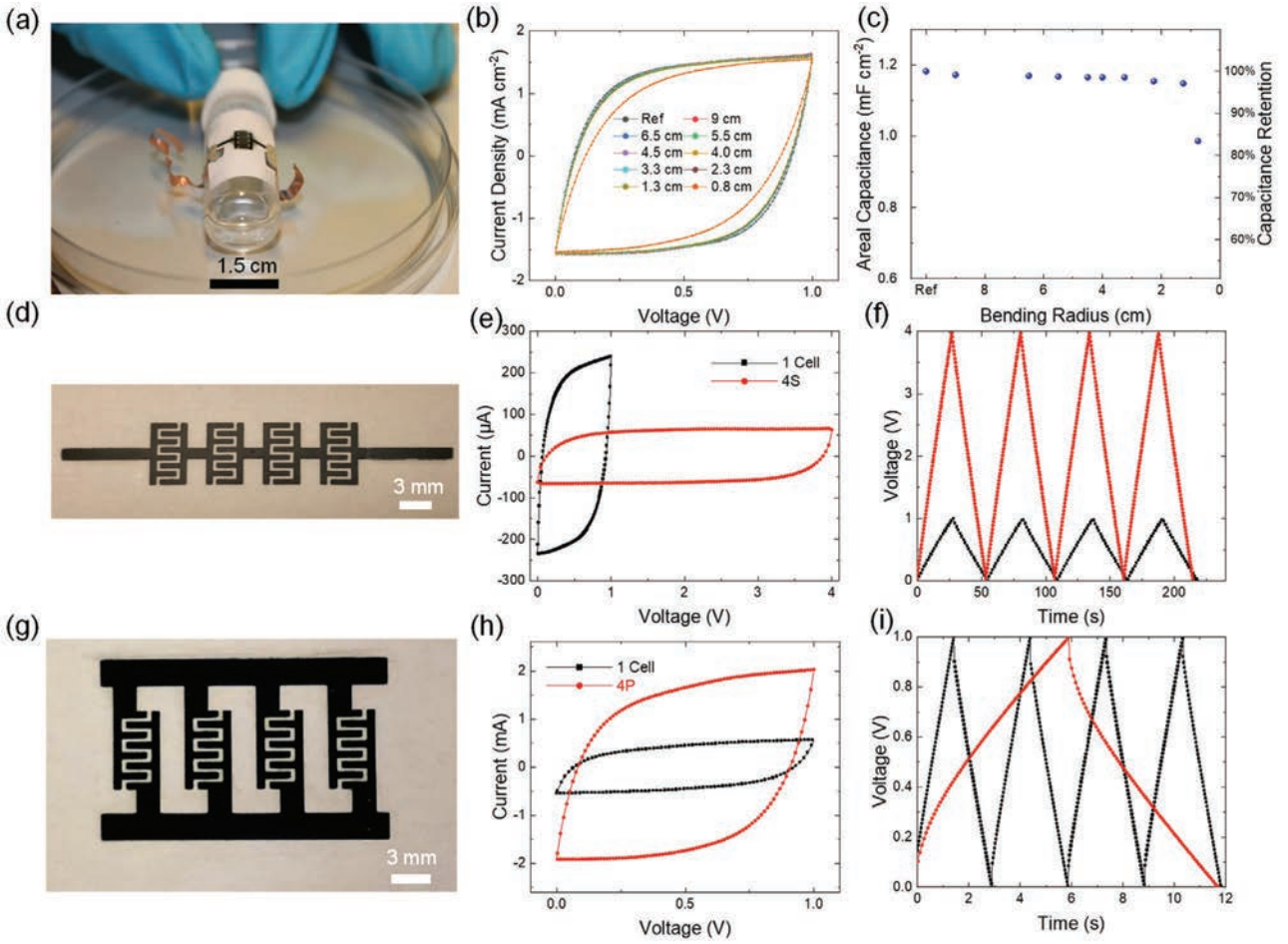

Figure 4. a) Photograph of a MSC printed on photo paper for flexibility performance test, b) the CV curves at 1000 mV s^{-1} and c) areal capacitance of the MSC under different mechanic bending radii, d) photograph of a fully-printed MSC array with four MSCs connected in series on carton paper, e) the CV curves at 1000 mV s^{-1} and f) GCD curves at 10 μA of the series-connection MSC array, g) photograph of a fully-printed MSC array with four MSCs connected in parallel on carton paper, h) the CV curves at 1000 mV s^{-1} and i) GCD curves at 200 μA of the parallel-connection MSC array. All the MSCs are printed with 10 passes. In (g), the bus lines are printed with 17 passes.

that the characteristic frequency (at a phase angle of −45°) of the equivalent resistor-capacitor circuits is about 3 Hz, implying faster frequency response than normal supercapacitors (about 1 Hz).[35] Finally, the largest volumetric capacitance of our MSCs has reached 3.1 F cm^{-3} at a scan rate of 1000 mV s^{-1}, which is comparable to that of the best devices/electrode materials in the literature (Table S2, Supporting Information), even including those with metal current collectors, liquid electrolyte, and/or very thin electrodes. As shown in Figure S7d,e, Supporting Information, the volumetric capacitance of our MSCs only has little dependence on the electrode thickness studied in this work. All these should be considered advantageous in view of the solid-state electrolytes and the lack of metal current collectors in the on-paper MSCs.

Additionally, the on-paper MSCs exhibit excellent mechanical flexibility (**Figure 4**a). As shown in Figure 4b, the CV curves of a 10-pass MSC were measured at a high scan rate of 1000 mV s^{-1} under various bending mechanical strains, with the curvature radii decreasing from 9 to 0.75 cm. Compared with the unstrained state (as the reference), the CV curves under strain states nearly remained unaltered when the curvature radius is larger than 1 cm (Figure 4b). Accordingly, the areal capacitance was almost invariant, just decreasing from 1.18 mF cm^{-2} under the unstrained state to 1.14 mF cm^{-2} at the small curvature radius of 1.25 cm (Figure 4c). Even at the very small curvature radius of 0.75 cm, still more than 80% of the reference capacitance can be retained. Also, when a 5-pass MSC is "folded" at a large angle of 70°, the capacitance is only degraded to 75% of the initial value (Figure S13, Supporting Information). These results prove the great potential of the on-paper MSCs for flexible electronics.

The practical applications often require series and/or parallel connections of individual MSCs to obtain sufficient voltage and current to power electronics. Although a large number of studies have successfully demonstrated the series and parallel connections of various MSCs at different scale, all of them still rely on external metal interconnects, which greatly reduces the scalability and disposability. In this work, we use inkjet printed PDG interconnects to connect 4 on-paper MSCs (with 10-pass electrodes) in series (Figure 4d) or in parallel (Figure 4g). Thanks to the high conductance of the printed PDG interconnects, the "totally metal-free MSC arrays" can be charged at

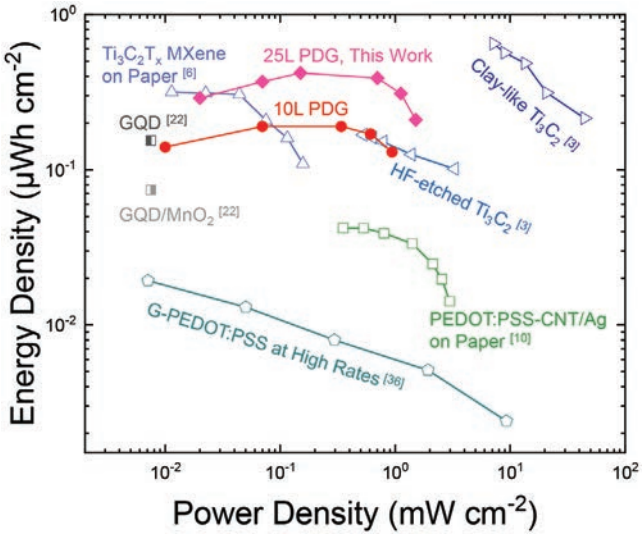

Figure 5. Areal Ragone plot for the state-of-the-art on-paper MSCs, and PEDOT:PSS- and GQD-based MSCs.

the high scan rate of 1000 mV s^{-1} with ideally rectangular CV curves (Figure 4e,h). Also, the series-connection (Figure 4f) and parallel-connection (Figure 4i) MSCs can be charged with triangular GCD curves at the current of 10 and 200 μA (corresponding to the high current density of 50 and 1000 μA cm^{-2} with respect to individual devices), respectively. This paves the way for practical applications of the high-rate on-paper MSCs in disposable electronics.

Areal energy density and areal power density are the key performance indicators for MSCs.[5] The areal Ragone plot in **Figure 5** compares the performance of our on-paper MSCs with the state-of-the-art on-paper MSCs, as well as MSCs based on similar electrode materials, in the literature.[3,6,10,22,36] Our MSCs exhibit a high areal energy density of 0.39 μWh cm^{-2} at the areal power density of 0.7 mW cm^{-2}. Even at the high areal power density of 1.5 mW cm^{-2}, the areal energy density is still as high as 0.21 μWh cm^{-2}. Clearly, our devices outperform most on-paper MSCs, even including the extrusion-printed all MXene MSCs.[6] The performance is even comparable to many MSCs with metal current collectors on rigid substrates (Table S3, Supporting Information). Although our PDG-based MSCs have inferior areal performance to the clay-like MXene-based MSCs,[3] the life cycle assessment (LCA) study (**Figure 6**a,b) indicates that their ecotoxicity and global warming potential (GWP) are much lower than the latter, no matter whether the full devices or individual components (electrodes or electrolytes) are considered. For more fair comparison, the ecotoxicity and GWP are normalized over the maximum energy of the devices. Figure 6c shows that with respect to the entire devices, our PDG-based MSCs have higher normalized ecotoxicity than the clay-like MXene MSCs. But this is mainly ascribed to the electrolyte part whereas our PDG electrodes themselves still have comparable normalized ecotoxicity to the MXene electrodes. In contrast, the PDG-based MSCs have

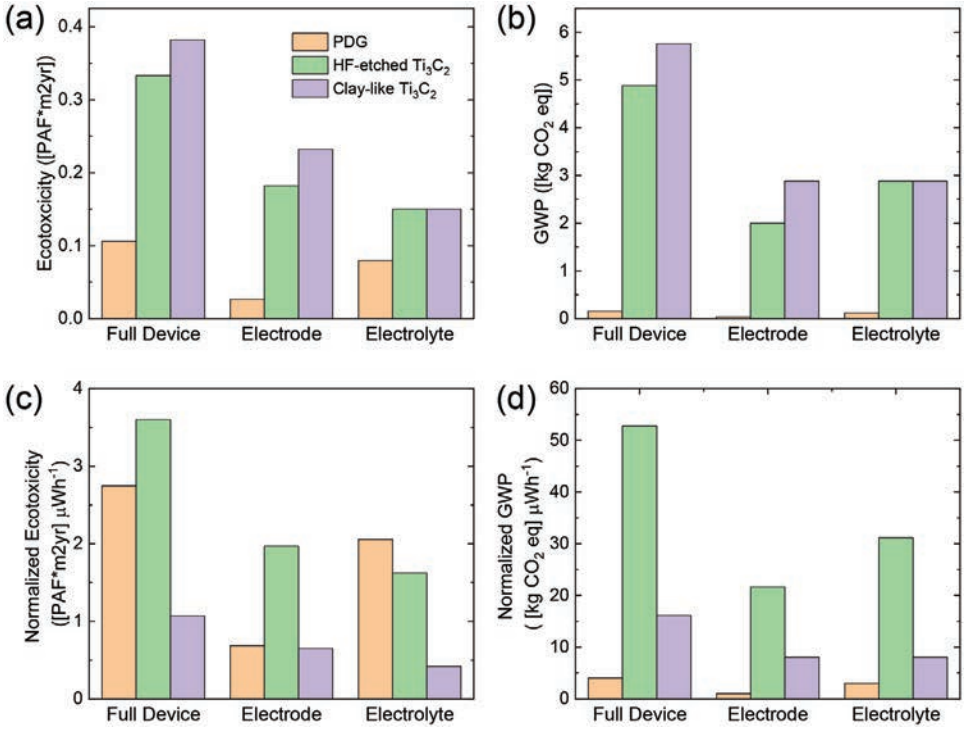

Figure 6. Life cycle assessment results for the PDG MSCs (10 printing passes) and MXene-based on-paper MSCs in Ref. [3]. a) Ecotoxicity, b) global warming potential (GWP), c) normalized ecotoxicity, and d) normalized GWP for the three kinds of on-paper MSCs in consideration of full device, electrode (including paper substrate and current collectors), and only electrolyte, respectively. In (c,d), the normalization is over the maximum energy that can be stored by the MSCs.

significantly lower normalized GWP than the MXene-based MSCs (Figure 6d). These confirm the superior eco-friendliness of the PDG-based MSCs.

3. Conclusion

In this work, we have found that a specific type of graphene quantum dots and electrochemically exfoliated graphene can synergistically stabilize PEDOT:PSS in water/ethylene glycol mixture solvent (with a largely negative zeta potential of −55 mV) to enable facile formulation of highly stable binder-free and metal-free conductive inks for reliable and scalable inkjet printing. It is feasible to print the inks at a small drop spacing of 10 µm to effectively produce large thickness (up to 9 µm, at the speed of ≈0.4 µm per pass) and meanwhile high resolution (critical size ≈ 300 µm). Without any post treatment, the printed metal-free patterns can attain a sheet resistance as low as 4 $\Omega\,\square^{-1}$ on paper substrates. The metal-free and all-solid-state paper MSCs can achieve areal capacitance > 2 mF cm^{-2} at a high scan rate of 1000 mV s^{-1}. The devices exhibit excellent cycle life (>95% capacitance retention after 10 000 cycles at a high scan rate of 1000 mV s^{-1} and large current density of 500 µA cm^{-2}), flexibility (≈95% capacitance retention at the bending radius of 1.25 cm) and long service life (no performance degradation after 2 months, without encapsulation). Moreover, the conductive inks also allow the direct printing of interconnect to connect four MSCs in series or in parallel on paper substrates to produce "totally metal-free" MSC arrays that can also be charged at a high scan rate of 1000 mV s^{-1} with scalable capacitance. In addition, our inkjet printed MSCs exhibit superior eco-friendliness to other high-performance on-paper MSCs. The printing technique is expected to expedite the practical application of paper MSCs to essentially contribute to disposable electronics.

4. Experimental Section

Material Synthesis: The GQDs were synthesized by pyrolysis of citric acid according to a protocol previously reported.[25,37] Briefly, 2 g of citric acid was placed in a beaker and heated to 220 °C until it turned from solid to colorless liquid in the first stage and gradually to pale orange. The orange liquid was added dropwise into 50 mL of 0.25 M NaOH solution under vigorous stirring. After cooled to room temperature, the obtained GQD were purified in a dialysis bag (retained molecular weight: 3500 Da) for 1 day to remove salt, unreacted citric acid and side-products. The dialyzed GQD solution was freeze-dried and the resulting GQD were stored dry. The EEG was synthesized with the same electrochemical exfoliation process introduced in the authors' previous work[14] to obtain stable EEG dispersion in dimethylformamide (DMF) at the concentration of ≈2 mg mL^{-1}.

PDG Ink Formulation: First, 1 mL EEG/DMF dispersion was centrifuged at 3000 rpm for 5 min to remove large particles, and the harvested 0.8 mL supernatant was further centrifuged at 13 000 rpm for 10 min to separate the EEG nanosheets from DMF. After the DMF supernatant was discarded, 0.7 mL commercially available PEDOT:PSS (1.1 wt%, Product No. 739 332, Sigma-Aldrich) was mixed with the EEG sediment and sonicated for 10 min to obtain the PEDOT:PSS/EEG dispersion. Then, 2 mg GQD was dispersed in 0.9 mL deionized water, added to PEDOT:PSS/EEG dispersion, and sonicated for 10 min. The ternary PDG dispersion was centrifuged at 3000 rpm for 10 min. Afterwards, 1.2 mL supernatant was harvested and mixed with 0.6 mL EG to obtain the final PDG ink. Roughly, the PDG ink comprises 3 mg mL^{-1} PEDOT:PSS, 0.1 mg mL^{-1} EEG, and 0.8 mg mL^{-1} GQD. The concentration of EEG is estimated from UV–vis spectra (Figure S14, Supporting Information).

MSC Fabrication: The fabrication only consists of two steps, printing of electrodes and drop casting of electrolytes. For electrode printing, the PDG inks were printed with the Dimatix Materials Printer (DMP 2800, FujiFilm Inc.) equipped with 10 pL cartridges (DMC-11610) on commercial Staples photo paper or Korsnäs carton paper, with the following parameters: drop spacing of 10 µm, on-printing substrate temperature of 40 °C and inter-print delay of 5–10 min. The ink was allowed to dry before printing the subsequent layer to avoid deformation of the paper substrates. The finally printed patterns were naturally dried in air. For electrolyte casting, each MSC is drop cast with 15 µL PSSH/H_3PO_4 electrolyte. The electrolyte is a simple mixture of 0.5 mL PSSH ($M_w \approx 75\,000$, 18 wt% in H_2O, Sigma-Aldrich, product number: 561 223) and 0.14 mL H_3PO_4 (≥85%, Sigma-Aldrich, product number: 40 278). After the electrolytes were dried in fume hood overnight, the MSCs were ready for electrochemical characterization.

Electrochemical Characterization: Silver paste was applied to each lead of the MSCs for external connection. All the electrochemical measurements, including CV, GCD, and EIS were performed at two-terminal configuration with the Gamry Interface 1010E potentiostat (Gamry Instruments Inc., Warminster PA, USA) connected with a Signatone S-1160 probe station equipped with S-725-PRM micropositioners (Signatone Corporation, Gilroy CA, USA). All the areal capacitance in this work refers to device capacitance, and was calculated in the same way as in the previous work.[11,33] The device area, referring to the footprint area (including the inter-finger gaps), is about 21 mm^2 for each MSC.

Material Characterization: The zeta potential and particle size distribution of all the inks were measured by Dynamic Light Scattering meter (Zetasizer Nano-ZS ZEN 3600 from Malvern Instruments). The concentration in the tested inks is 10 times diluted, as compared with those listed in Table S1, Supporting Information. The UV–vis absorption spectra were measured with the UV–vis spectrophotometer (Jasco V-570 UV-VIS-NIR). The TEM analysis of the PDG inks was conducted in a JEOL JEM 2100 TEM with a LaB_6 cathode. The micrographs were recorded using a direct electron detector (model CheeTah1800, a Medipix3Rx based camera from Amsterdam Scientific Instruments, Netherlands) with a high dynamic range and high detective quantum efficiency compared to traditional phosphor-based electron detectors. The TEM samples were prepared through drop casting of ten times diluted PDG inks onto a carbon grid and drying in a fume hood.

Life Cycle Assessment: The LCA was performed through the software SimaPro with the inputs listed in Table S4, Supporting Information. The ecotoxicity and GWP were studied through the methods, ECO-indicator 99 (H) and IPCC 2013 GWP 100a, respectively.

Supporting Information

Supporting Information is available from the Wiley Online Library or from the author.

Acknowledgements

The authors acknowledge the financial support from the Formas Foundation through the Future Research Leaders Grant (No. 2016-00496), the ÅForsk Foundation (Grant No. 17-352), the Swedish Research Council (Grant No. 2019-04731), the Olle Engkvist Byggmästare Foundation (Grant No. 2014/799), and the Swedish Foundation for International Cooperation in Research and Higher Education (STINT, CH2017-7284).

Conflict of Interest

The authors declare no conflict of interest.

Data Availability Statement

The data that support the findings of this study are available from the corresponding author upon reasonable request.

Keywords

disposable electronics, electrochemically exfoliated graphene, graphene quantum dots, inkjet printing, on-paper microsupercapacitors, PEDOT:PSS

Received: August 31, 2021
Revised: October 7, 2021
Published online: October 22, 2021

[1] S. Nandy, S. Goswami, A. Marques, D. Gaspar, P. Grey, I. Cunha, D. Nunes, A. Pimentel, R. Igreja, P. Barquinha, L. Pereira, E. Fortunato, R. Martins, *Adv. Mater. Technol.* **2021**, *6*, 2000994.
[2] X. Aeby, A. Poulin, G. Siqueira, M. K. Hausmann, G. Nyström, *Adv. Mater.* **2021**, *33*, 2101328.
[3] N. Kurra, B. Ahmed, Y. Gogotsi, H. N. Alshareef, *Adv. Energy Mater.* **2016**, *6*, 1601372.
[4] X. Zang, C. Shen, Y. Chu, B. Li, M. Wei, J. Zhong, M. Sanghadasa, L. Lin, *Adv. Mater.* **2018**, *30*, 1800062.
[5] N. A. Kyeremateng, T. Brousse, D. Pech, *Nat. Nanotechnol.* **2017**, *12*, 7.
[6] C. Zhang, L. McKeon, M. P. Kremer, S.-H. Park, O. Ronan, A. Seral-Ascaso, S. Barwich, C. Ó. Coileáin, N. McEvoy, H. C. Nerl, B. Anasori, J. N. Coleman, Y. Gogotsi, V. Nicolosi, *Nat. Commun.* **2019**, *10*, 1795.
[7] Y. Xia, T. S. Mathis, M.-Q. Zhao, B. Anasori, A. Dang, Z. Zhou, H. Cho, Y. Gogotsi, S. Yang, *Nature* **2018**, *557*, 409.
[8] S. Lin, J. Tang, K. Zhang, T. S. Suzuki, Q. Wei, M. Mukaida, Y. Zhang, H. Mamiya, X. Yu, L.-C. Qin, *J. Power Sources* **2021**, *482*, 228995.
[9] R. Guo, J. Chen, B. Yang, L. Liu, L. Su, B. Shen, X. Yan, *Adv. Funct. Mater.* **2017**, *27*, 1702394.
[10] W. Liu, C. Lu, H. Li, R. Y. Tay, L. Sun, X. Wang, W. L. Chow, X. Wang, B. K. Tay, Z. Chen, J. Yan, K. Feng, G. Lui, R. Tjandra, L. Rasenthiram, G. Chiu, A. Yu, *J. Mater. Chem. A* **2016**, *4*, 3754.
[11] J. Li, F. Ye, S. Vaziri, M. Muhammed, M. C. Lemme, M. Östling, *Adv. Mater.* **2013**, *25*, 3985.
[12] S. Sollami Delekta, M.-M. Laurila, M. Mäntysalo, J. Li, *Nano-Micro Lett.* **2020**, *12*, 40.
[13] J. Liang, C. Jiang, W. Wu, *Appl. Phys. Rev.* **2021**, *8*, 021319.
[14] J. Li, S. Sollami Delekta, P. Zhang, S. Yang, M. R. Lohe, X. Zhuang, X. Feng, M. Östling, *ACS Nano* **2017**, *11*, 8249.
[15] G. Cai, P. Darmawan, M. Cui, J. Wang, J. Chen, S. Magdassi, P. S. Lee, *Adv. Energy Mater.* **2016**, *6*, 1501882.
[16] T. Cheng, Y.-Z. Zhang, J.-P. Yi, L. Yang, J.-D. Zhang, W.-Y. Lai, W. Huang, *J. Mater. Chem. A* **2016**, *4*, 13754.
[17] E. Bihar, T. Roberts, M. Saadaoui, T. Hervé, J. B. De Graaf, G. G. Malliaras, *Adv. Healthcare Mater.* **2017**, *6*, 1601167.
[18] Y. Wang, Y.-Z. Zhang, D. Dubbink, J. E. ten Elshof, *Nano Energy* **2018**, *49*, 481.
[19] Y.-Z. Zhang, Y. Wang, T. Cheng, L.-Q. Yao, X. Li, W.-Y. Lai, W. Huang, *Chem. Soc. Rev.* **2019**, *48*, 3229.
[20] L.-W. Lo, J. Zhao, H. Wan, Y. Wang, S. Chakrabartty, C. Wang, *ACS Appl. Mater. Interfaces* **2021**, *13*, 21693.
[21] X. Fan, W. Nie, H. Tsai, N. Wang, H. Huang, Y. Cheng, R. Wen, L. Ma, F. Yan, Y. Xia, *Adv. Sci.* **2019**, *6*, 1900813.
[22] W.-W. Liu, Y.-Q. Feng, X.-B. Yan, J.-T. Chen, Q.-J. Xue, *Adv. Funct. Mater.* **2013**, *23*, 4111.
[23] W. Liu, M. Li, G. Jiang, G. Li, J. Zhu, M. Xiao, Y. Zhu, R. Gao, A. Yu, M. Feng, Z. Chen, *Adv. Energy Mater.* **2020**, *10*, 2001275.
[24] J. Li, M. C. Lemme, M. Östling, in *Nanomaterials for 2D and 3D Printing* (Eds: S. Magdassi, A. Kamyshny), Wiley-VCH, Weinheim, Germany **2017**, p. 161.
[25] V. Ruiz, I. Fernández, P. Carrasco, G. Cabañero, H. J. Grande, J. Herrán, *Sens. Actuators, B* **2015**, *218*, 73.
[26] A. Kumar, C. K. Dixit, in *Advances in Nanomedicine for the Delivery of Therapeutic Nucleic Acids* (Eds: S. Nimesh, R. Chandra, N. Gupta), Woodhead Publishing, Sawston, Cambridge **2017**, p. 43.
[27] F.-P. Du, N.-N. Cao, Y.-F. Zhang, P. Fu, Y.-G. Wu, Z.-D. Lin, R. Shi, A. Amini, C. Cheng, *Sci. Rep.* **2018**, *8*, 6441.
[28] K. Parvez, Z.-S. Wu, R. Li, X. Liu, R. Graf, X. Feng, K. Müllen, *J. Am. Chem. Soc.* **2014**, *136*, 6083.
[29] M. Kuang, L. Wang, Y. Song, *Adv. Mater.* **2014**, *26*, 6950.
[30] E. B. Secor, B. Y. Ahn, T. Z. Gao, J. A. Lewis, M. C. Hersam, *Adv. Mater.* **2015**, *27*, 6683.
[31] O. Larsson, E. Said, M. Berggren, X. Crispin, *Adv. Funct. Mater.* **2009**, *19*, 3334.
[32] N. Anjum, N. Joyal, J. Iroegbu, D. Li, C. Shen, *J. Power Sources* **2021**, *499*, 229962.
[33] V. Mishukova, N. Boulanger, A. Iakunkov, S. Sollami Delekta, X. Zhuang, A. Talyzin, J. Li, *Nanoscale Adv.* **2021**, *3*, 4674.
[34] M. F. El-Kady, R. B. Kaner, *Nat. Commun.* **2013**, *4*, 1475.
[35] J. R. Miller, R. A. Outlaw, B. C. Holloway, *Science* **2010**, *329*, 1637.
[36] Z.-S. Wu, Z. Liu, K. Parvez, X. Feng, K. Müllen, *Adv. Mater.* **2015**, *27*, 3669.
[37] Y. Dong, J. Shao, C. Chen, H. Li, R. Wang, Y. Chi, X. Lin, G. Chen, *Carbon* **2012**, *50*, 4738.